J Mater Sci (2020) 55:6417–6428

Ceramics

Low-temperature thermophysical and crystallographic properties of $BaZrO_3$ perovskite

K. S. Knight[1,2,*]

[1] Department of Earth Sciences, The Natural History Museum, Cromwell Road, London SW7 5BD, UK
[2] Department of Earth Sciences, University College London, Gower Street, London WC1E 6BT, UK

Received: 20 November 2019
Accepted: 10 February 2020
Published online: 21 February 2020

ABSTRACT

The temperature dependence of the crystallographic and thermoelastic properties of $BaZrO_3$ perovskite in the temperature range 4.2 K and 450 K has been investigated using high-resolution time-of-flight neutron powder diffraction and literature values of the isobaric heat capacity. At all measured temperatures, $BaZrO_3$ is cubic, space group $Pm\bar{3}m$, with no clear evidence for diffuse scattering at critical points of the primitive cubic Brillouin zone. Simultaneous fitting of the temperature dependences of the isochoric heat capacity and unit cell volume showed the thermophysical properties of $BaZrO_3$ were consistent with a two-term Debye model in which the cations and anions behave independently of one another with Debye temperatures of 220(2) K and 730(5) K, respectively. This model is further consistent with the temperature variations of the atomic displacement parameters fitted to a modified Debye model in which the vibrational Debye temperatures of the anion are significantly larger than those associated with the cations. The evolution of the crystallographic parameters of $BaZrO_3$ is compared to those of $BaCeO_3$, for barium in the cavity site, and $SrZrO_3$, for zirconium in the octahedral site.

Introduction

Barium zirconate, $BaZrO_3$, is a perovskite-structured compound [1] that crystallises with the aristotype [2] crystal structure in space group $Pm\bar{3}m$ in the temperature range 4.2 K [3] to 1700 K [4]. $BaZrO_3$ is a well-studied ceramic oxide due to a number of technologically useful properties: as a high-temperature proton or oxide ion conductor when aliovalent cations are substituted for zirconium [5–7], and as a component of lead-free piezoelectrics [8]. In addition, the high-temperature behaviour of $BaZrO_3$ has been studied as an easily synthesised clone phase of bridgmanite ($MgSiO_3$ perovskite) to infer behaviour of the Earth's lower mantle [9]. The presence of $BaZrO_3$ in solid solution with other perovskite-structured materials in fission product compounds in uranium–plutonium mixed oxide fuels in fast breeder reactors has led to a significant number of investigations of its high-temperature thermophysical properties including calorimetry, thermal

Address correspondence to E-mail: kevinstevenknight@gmail.com

https://doi.org/10.1007/s10853-020-04453-5

conductivity, microhardness and elastic moduli [4, 10–15].

Despite the evidence from low-temperature neutron diffraction measurements that show $BaZrO_3$ is cubic below 10 K [3, 6] with no evidence for superlattice reflections or diffuse scattering at the R or M points of the Brillouin zone, ab initio calculations have shown that an instability exists at the R point where the calculated phonons exhibit negative frequencies [3, 16–18]. This instability is associated with a triply degenerate phonon with irreducible representation R_4^+ in which successive ZrO_6 octahedra along the cubic crystallographic axes rotate in an antiphase manner [19]. Results of first principles calculations carried out on $BaZrO_3$ are consistent with a single component of this mode condensing out giving rise to a lower symmetry tetragonal phase with space group $I4/mcm$ [3, 16–18]. The deduction that the theoretical ground state of $BaZrO_3$ is tetragonal, in conflict with crystallographic experiments, is not universally accepted, and the stabilisation of the cubic crystal structure due to quantum zero-point vibrations and anharmonic effects stabilising the soft modes has recently been proposed [20]. The effect of yttrium doping for zirconium in $BaZrO_3$ has been the subject of a synchrotron powder diffraction, EXAFS and Raman spectroscopic investigation with the conclusion that for $0.06 < x < 0.15$ in $BaZr_{1-x}Y_xO_{3-\delta}$ the crystal structure is tetragonal in space group $P4/mbm$ [21]. This would be consistent with a soft-mode transition associated with a phonon that transforms as the irreducible representation M_3^+ [19]. Consideration of Fig. 3 of reference [21] shows that no additional superlattice reflections are observed at the M point of the pseudocubic Brillouin zone when compared to the diffraction pattern of the undoped compound (reference [21] Fig. 2), although allowing the unit cell to become tetragonal is demonstrated from fitting of the 200 and 310 Bragg reflections. The quoted fractional coordinates of the anion O2 are simply those of the aristotype transformed to the tetragonal unit cell and hence would not give rise to the expected superlattice reflections. Furthermore, most ab initio calculations of the phonons in $BaZrO_3$ do not show that negative frequencies are associated with the M point, unlike the R point [3, 16–18], although the whole branch between the R and the M points is soft according to Bilić and Gale [20]. The deduced space group of $BaZr_{1-x}Y_xO_{3-\delta}$ is therefore open to debate. As a small tetragonal distortion has been proven to occur in $BaZr_{1-x}Y_xO_{3-\delta}$ for $0.06 < x < 0.15$, a high-resolution neutron powder diffraction investigation would be beneficial in confirming the structural characterisation of these materials as the appearance of the diagnostic superlattice reflections is principally dependent upon anion fractional coordinates in zone-boundary-tilted perovskite crystal structures.

Further experimental evidence for a lower crystallographic symmetry than the aristotype phase has been afforded by Raman spectroscopic investigations of $BaZrO_3$ [21, 22]. First-order Raman scattering is forbidden for the aristotype perovskite crystal structure; however, a strong Raman spectrum has been experimentally observed, suggesting the presence of localised structural distortions. Despite this, the spectra presented by Shi et al. [22] are not in detailed agreement with those of Giannici et al. [21], suggesting scope for further detailed vibrational spectroscopic investigations.

Whilst the true nature of the ground state of $BaZrO_3$ remains uncertain, cubic, tetragonal or tetragonal without long-range order, a high-pressure phase transition at 17.2 GPa to a long-range ordered tetragonal phase in space group $I4/mcm$ has been observed experimentally [23].

In the work to be presented here, we report the first detailed crystallographic and thermoelastic study of $BaZrO_3$ at ninety temperatures between 4.2 and 450 K. We demonstrate that at low to intermediate temperatures, $BaZrO_3$ perovskite can be treated thermodynamically in a simple self-consistent two-term Debye model [24–26].

Method

Neutron powder diffraction data were collected in time-of-flight using the long-flightpath, high-resolution, backscattering powder diffractometer (HRPD) of the ISIS Facility, Rutherford Appleton Laboratory. The advantage of this instrument over constant wavelength instrumentation is that to first order, the resolution function is independent of scattering vector ($Q = 4\pi\sin(\theta)/\lambda$), and hence, $\Delta d/d$ is approximately constant over the whole diffraction pattern. This almost constant Q resolution reduces Bragg reflection overlap in a powder diffraction pattern and hence permits the detailed characterisation of two

compounds as a mixture under the identical thermodynamic conditions providing the unit cell metrics are well separated. The methodology has been exploited in temperature-dependent crystallographic studies of $LaGaO_3$ [24] and $SrZrO_3$ [25], and $BaCeO_3$ [26] and $SrCeO_3$ [Knight and Bonanos, in preparation] mixtures. In the work to be described below, we have studied a mixture of two cubic perovskite-structured phases, $BaZrO_3$ and $KTaO_3$, and described the evolution of thermophysical and crystallographic properties of the zirconate phase; results derived from the analysis of the tantalate compound will be described elsewhere. For this mixture, there was no appreciable Bragg peak overlap in the backscattering data between the two phases at any of the measured temperatures.

5.428 g of commercially synthesised $BaZrO_3$ powder (Sigma-Aldrich) was annealed at 1773 K under air for 24 h and then intimately mixed with 5.261 g of $KTaO_3$ powder (Sigma-Aldrich) using an agate pestle and mortar. The equimolar admixture was located into a directly heated 1.5-cm-thick aluminium sample can of slab geometry equipped with thin vanadium windows. Specifics of this sample geometry, thermometry and thermal stability have recently been described in detail by Fortes [27] and will not be elaborated on further in this publication. The can was cooled to 4.2 K using an AS Scientific 'Orange' cryostat and was then equilibrated for 1 h. Neutron time-of-flight data were then collected in the time-of-flight window 30–130 ms at 4.2 K for 6 μAh, approximately 9 min duration, before the sample was heated to the next temperature, 10 K. To ensure thermal equilibration was achieved, the sample was required to reach the set-point temperature before a 5-min equilibration period was commenced. Data were then collected for 6 μAh and the temperature increased by 5 K, with the whole protocol of heating, equilibration and data collection being repeated up to 445 K. Finally, the sample was heated to 450 K and equilibrated, and data were collected for 40 μAh, approximately 1 h of duration; this procedure was repeated in 50 K steps on cooling to 150 K, then to 75 K and finally at 4.2 K. For all measurements, the temperature variation was better than ± 0.2 K of the set-point temperature.

The neutron time-of-flight data were focused, normalised to the incident flux distribution and corrected for solid angle variation. These data were then further corrected for self-shielding for a sample of nominal composition $(BaK)_{0.5}(ZrTa)_{0.5}O_3$, number density of 4.63×10^{21} cm^{-3}, scattering cross section of 21.6 b [28] and wavelength-dependent absorption for an absorption cross section of 12.0 b at a wavelength of 1.798 Å [28]. Data sets were generated in GSAS [29] format in the time-of-flight range 32–120 ms that corresponds to a d-spacing range of 0.66–2.48 Å for the high-resolution backscattering bank and 0.92–3.44 Å in the high-count-rate 90° detector bank.

Data analysis

Multibank, multiphase crystal structure refinement was performed using the GSAS software suite [29] for a crystallographic model with isotropic atomic displacement parameters for the cations and anisotropic thermal parameters for the anion. Data analysis commenced with the 4.2 K run, which, once converged, formed the starting model for the 10 K run; the refinement process was iterated up to the 450 K measurement. As the crystallographic refinement was facile due to both phases containing atoms in special (fixed) positions in space group $Pm\bar{3}m$ (see Table 1), convergence was rapid with typical agreement factors of Rp = 0.065, Rwp = 0.078, $\chi^2 = 2.4$ for a model with 35 parameters (1 phase fraction, 2 scale factors, 2 lattice parameters, 4 cation isotropic atomic displacement parameters, 4 anion anisotropic atomic displacement parameters, 12 peak shape parameters and 10 background terms). The phase fraction refined to 0.504(2) in excellent agreement with that expected from the individual component masses (0.5). Refinement of the site occupancy factors of all atoms was introduced into the 4.2 K refinement and showed the expected stoichiometry within one estimated standard deviation. All subsequent refinements were hence carried out assuming an ideal composition of $BaZrO_3$. Average estimated standard deviations for the structural parameters of $BaZrO_3$ in the short data collection times were 1.5×10^{-5} Å for the lattice parameter, 4×10^{-4} $Å^2$ and 3×10^{-4} $Å^2$ for the barium and zirconium isotropic temperature factors, respectively, and 7×10^{-4} $Å^2$ and 4×10^{-4} $Å^2$ for the oxygen anisotropic atomic displacement terms u_{11} and u_{33} (= u_{22}). The quality of fit to these data is illustrated in Fig. 1 for the 4.2 K measurement, and the refined structural parameters for the nine long runs are listed in Table 1.

Table 1 Crystallographic parameters for $BaZrO_3$ at selected temperatures

Temperature/K	450	400	350	300	250	200	150	75	4.2
Lattice parameter/Å	4.19698(1)	4.19555(1)	4.19421(1)	4.19294(1)	4.19179(1)	4.19074(1)	4.18983(1)	4.18878(1)	4.18845(1)
100 Ba u_{iso}/Å^2	1.11(3)	1.01(3)	0.91(3)	0.83(3)	0.68(3)	0.60(3)	0.50(3)	0.37(3)	0.27(3)
100 Zr u_{iso}/Å^2	0.98(2)	0.93(2)	0.88(2)	0.83(2)	0.78(2)	0.75(2)	0.71(2)	0.69(2)	0.65(3)
100 O u_{11}/Å^2	1.00(5)	0.96(5)	0.93(5)	0.92(5)	0.83(5)	0.87(5)	0.87(6)	0.87(6)	0.83(6)
100 O u_{33}/Å^2	1.94(3)	1.81(3)	1.64(3)	1.48(3)	1.34(3)	1.17(3)	1.05(3)	0.89(3)	0.82(3)
Rp	0.036	0.035	0.036	0.036	0.037	0.037	0.037	0.040	0.042
Rwp	0.056	0.056	0.056	0.059	0.059	0.060	0.060	0.063	0.067
χ^2	8.04	8.07	8.08	8.80	8.87	9.05	9.19	8.64	8.57

Space group:$Pm\bar{3}m$. Ba 1*b* (1/2 1/2 1/2), Zr 1*a* (0 0 0), O 3*d* (1/2 0 0)

No evidence for diffuse scattering was observed at the R point positions of the cubic Brillouin zone in the high-count-rate 90° 2θ data sets, the presence of which would support the conclusions of some of the DFT calculations that the ground state of $BaZrO_3$ contains nanoclusters of lower symmetry. A single crystal neutron diffuse scattering of $BaZrO_3$ may shed further light on this conjecture.

Results

Lattice parameter, unit cell volume and characteristic temperatures

Figure 2 shows the temperature dependence of the lattice parameter of $BaZrO_3$ between 4.2 and 450 K. The temperature variation is as expected for a non-magnetic, dielectric material without structural phase transitions: saturation at low temperature, in this case for temperatures below $\sim$ 40 K, and a linear temperature dependence at higher temperatures, above $\sim$ 350 K. The smooth, monotonic variation, however, masks a subtle temperature variation. For many materials which do not undergo structural phase transitions, the temperature variation of the lattice constant(s) from liquid helium temperatures may be empirically fitted using an expression related to an Einstein internal energy function [30], $a(T) = a_0 + k_i/(\exp(E_i/T) - 1)$. However, in this case, although the lattice parameter data of $BaZrO_3$ superficially seem well fitted, the difference/e.s.d. (Δ/σ) showed a large systematic oscillatory discrepancy for temperatures below 200 K as illustrated in Fig. 2 by the dot–dash line (r^2 = 0.99909). Permitting

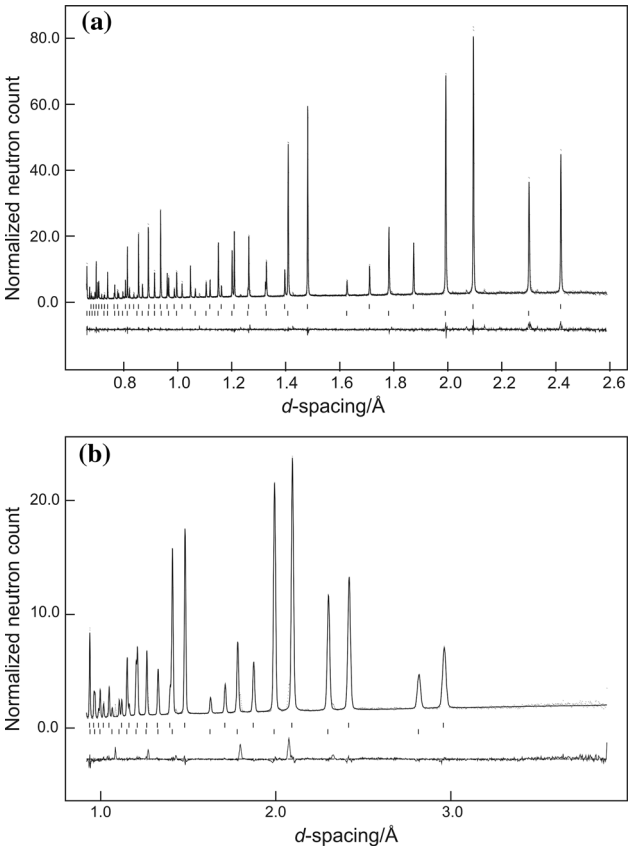

Figure 1 Profile refinement fit to the 4.2 K data collected on $BaZrO_3$ using the high-resolution time-of-flight powder diffractometer (HRPD). **a** Profile refinement fit to the high-resolution backscattering bank; **b** the simultaneous fit to the high-count-rate, medium-resolution 90° bank. Observed data are shown as points, the calculated pattern as the full line, and reflection markers are for $BaZrO_3$ (upper) and $KTaO_3$ (lower). The difference (observed–calculated) is shown as the full line below the reflection markers for $KTaO_3$.

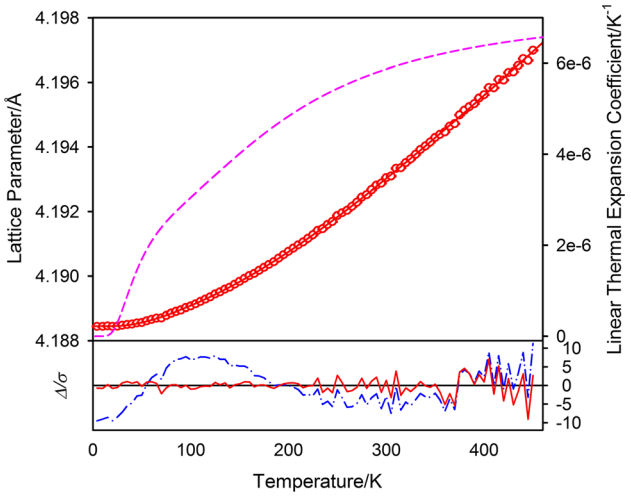

Figure 2 The temperature variation of the lattice parameter of $BaZrO_3$ between 4.2 and 500 K. The lower plot illustrates the difference/estimated standard deviation (Δ/σ) for the two models discussed in the text. The dot–dash line shows Δ/σ for the single-term model indicating a systematic misfit at low temperatures. The full line shows Δ/σ for the two-term model that exhibits no systematic misfit. The dashed line in the upper figure illustrates the linear thermal expansion coefficient calculated from the two-term fitting parameters.

a second temperature-dependent term to the fitting procedure resulted in the full line shown passing through the experimental lattice parameter data and the full line in the Δ/σ plot (r^2 = 0.99983). In this case, there is no systematic behaviour at low temperature and $|\Delta/\sigma|$ is less than 3 for all data below 350 K. The fitting parameters for the lattice parameter are listed in Table 2.

The linear thermal expansion coefficient (α_L) for $BaZrO_3$ was calculated using the fitting parameters and is illustrated in Fig. 2 as the dashed line. α_L varies from ~ 0 at 4.2 K, increasing monotonically to $\sim 3.0 \times 10^{-6}$ K^{-1} by 100 K before showing an approximately linear temperature dependence to 250 K (5.4×10^{-6} K^{-1}). Above this temperature, the rate of change of α_L with temperature reduces, reaching a value of 6.6×10^{-6} K^{-1} at 500 K. Based on the fitting coefficients, a high temperature value for α_L is estimated as 7.2×10^{-6} K^{-1}. The sub-300 K results are in fair agreement with the average value of α_L derived from two points measured by neutron powder diffraction at 100 and 300 K (4.7×10^{-6} K^{-1}) [3]. The estimated high-temperature limit is consistent with high-temperature experimental results derived from X-ray diffraction (6.87×10^{-6} K^{-1} [9], 7.5×10^{-6} K^{-1} [31], 8.02×10^{-6} K^{-1} [32], 7.89×10^{-6} K^{-1} [33]) and dilatometry (7.13×10^{-6} K^{-1} [12]).

Table 2 Refined fitting parameters for the temperature dependence of the lattice parameter of $BaZrO_3$

Parameter	
a_0/Å	4.18845(1)
k_1/Å	0.0022(2)
E_1/K	151(6)
k_2/Å	0.0108(2)
E_2/K	683(20)

In contradistinction to the fitting of the lattice parameter to an empirical function of temperature, the temperature dependence of the unit cell volume can be fitted to a variety of statistical mechanical models on the assumption of a Grüneisen approximation to the zero-pressure equation of state. To the first order, the volume will vary as the internal energy ($U(T)$); $V(T) = V_0 + (\gamma/K_0)U(T)$ [34] where γ is a Grüneisen parameter and K_0 is the isothermal bulk modulus. Furthermore, as the isochoric heat capacity (c_V) is the temperature derivative of the internal energy function at constant volume, a self-consistent solution may be found by fitting the unit cell volume and the isochoric heat capacity simultaneously to the same internal energy function. An Einstein model for the internal energy function with a delta function in the phonon density of states is clearly an over-simplification, and hence, we have used a more realistic Debye model. For this model of the internal energy function, the volume and the isochoric heat capacity as a function of temperature are given by the expressions [30]

$$V(T) = V_0 + \frac{9\gamma N k_B T}{K_0}\left(\frac{T}{\theta_D}\right)^3 \int_0^{\theta_D/T} \frac{x^3 dx}{e^x - 1}$$

$$c_V(T) = 9Nk_B T\left(\frac{T}{\theta_D}\right)^3 \int_0^{\theta_D/T} \frac{x^4 e^x dx}{(e^x - 1)^2}$$

where N is the number of atoms, k_B is Boltzmann's constant and θ_D is the Debye temperature.

The temperature dependence of the unit cell volume is illustrated as the upper graph in Fig. 3. Preliminary fitting of the unit cell volume to the Debye internal energy function found the identical systematic discrepancy in the Δ/σ plot that was observed when fitting the lattice parameter to the single-term energy function. This is not unexpected as the Debye temperature derived from heat capacity data is generally temperature dependent [30]. Within the simple model for $BaZrO_3$ we are proposing, the discrepancy in Δ/σ indicated the necessity of applying a second

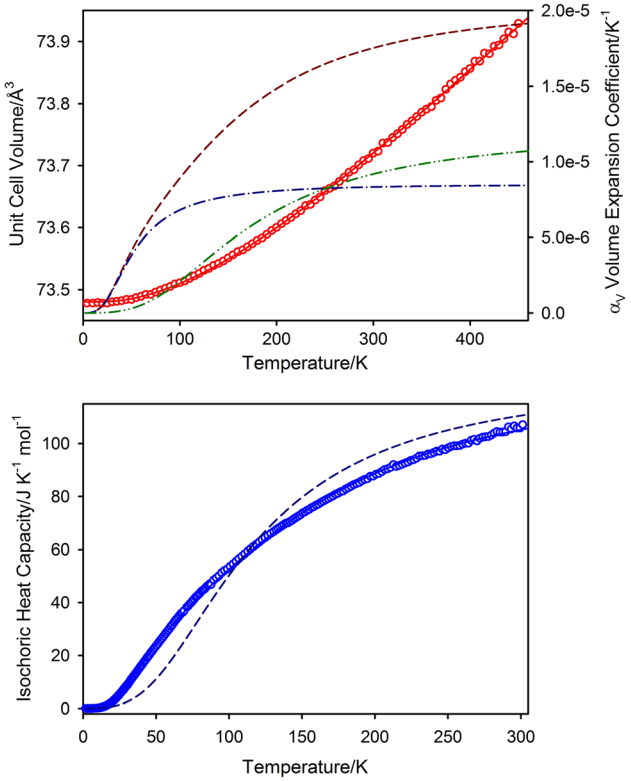

Figure 3 The simultaneous fit to the unit cell volume (upper) and isochoric heat capacity (lower) for $BaZrO_3$ using the two-term Debye model described in the text: circles data, full line fit to these data. The dashed line in the upper figure illustrates the volume expansion coefficient calculated using the fitting coefficients. The dot–dash line shows the contribution of the lower Debye temperature term to the volume expansion coefficient, and the upper shows the contribution from the higher Debye temperature. The dashed line in the lower figure illustrates the inadequacy of the single-term Debye model to fit the isochoric heat capacity.

temperature-dependent term to both functions. The volume and isochoric heat capacity are then given by

$$V(T) = V_0 + z\frac{9\gamma_1 N k_B T}{K_0}\left(\frac{T}{\theta_{D1}}\right)^3 \int_0^{\theta_{D1}/T} \frac{x^3 dx}{e^x - 1} + (1-z)\frac{9\gamma_2 N k_B T}{K_0}\left(\frac{T}{\theta_{D2}}\right)^3 \int_0^{\theta_{D2}/T} \frac{x^3 dx}{e^x - 1}$$

$$c_V(T) = 9zNk_B T\left(\frac{T}{\theta_{D1}}\right)^3 \int_0^{\theta_{D1}/T} \frac{x^4 e^x dx}{(e^x - 1)^2} + 9(1-z)Nk_B T\left(\frac{T}{\theta_{D2}}\right)^3 \int_0^{\theta_{D2}/T} \frac{x^4 e^x dx}{(e^x - 1)^2}$$

where z is a mixing parameter: $0 < z < 1$.

The molar isobaric heat capacity (c_P) for $BaZrO_3$ has been reported in the temperature interval 1.6–301.3 K at 375 temperatures [35], and these data have been converted to the isochoric form using the standard thermodynamic transformation $c_V = c_P - T\alpha_V^2 K_0 V_m$[30], where V_m is the molar volume and α_V is the volume expansion coefficient. In the absence of experimental results of the temperature variation of the bulk modulus of $BaZrO_3$, K_0 was considered to be a constant, 189 GPa, derived from the ambient temperature equation of state [23]. The volume expansivity and molar volume were calculated from fitting the unit cell volume to a simpler two-term Einstein model which was an adequate approximation for purposes of the transformation. The calculated isochoric heat capacity of $BaZrO_3$ is shown in the lower graph of Fig. 3.

The unit cell volume and the isochoric heat capacity were fitted simultaneously to the two-term Debye models shown above, originally with the mixing parameter z freely refined. The refinement of this parameter did not converge to 1/3 or 2/3, as would be consistent with Barron's model [36] that allows different cut-off frequencies for the longitudinal and transverse modes, but to $\sim$ 0.43 which is close to 0.4, the cation fraction in the formula unit. Setting this parameter to 0.4 made little difference to the agreement factors for fitting the two data sets, and hence, this value of the mixing parameter was retained, and we consider the two characteristic temperatures to be broadly related to separated cation and anion behaviour. The full lines on the upper and lower graphs of Fig. 3 show the fitted temperature dependences of the unit cell volume and isochoric heat capacity to the two-term Debye model (r^2 = 0.99939). The saturated unit cell volume, characteristic temperatures and Grüneisen constants (assuming K_0 = 189 GPa [23]) for the two-term Debye model are listed in Table 3. The weighted average of the two Debye temperatures, 526(1) K, shows good agreement with both ab initio calculation (525 K) [37], ultrasonic pulse echo technique (544 K) [13, 14], and calorimetry, for temperatures greater than $\sim$ 150 K, as illustrated in Fig. 3 of Ahrens and Maier [35]. The inadequacy of a single Debye term to simultaneously fit the heat capacity and volume data can be appreciated by the dashed line on the lower graph, for which the Debye temperature was refined as 471 K and the Grüneisen constant as 1.34.

The temperature dependence of the volume expansion coefficient of $BaZrO_3$ is shown as the dashed line in the upper graph of Fig. 3 with an

Table 3 Refined fitting parameters for the temperature dependence of the unit cell volume and isochoric heat capacity of $BaZrO_3$

Parameter	
V_0/Å^3	73.48(23)
γ_1	1.44
θ_{D1}/K	220(2)
γ_2	1.36
θ_{D2}/K	730(5)

estimated high-temperature limit of 2.0×10^{-5} K^{-1}; the individual contributions from the two Debye terms are shown as the dot–dash and dot–dot–dash lines. It can be seen that the contribution from the lower Debye temperature term reaches saturation (0.84×10^{-5} K^{-1}) by $\sim$ 200 K and hence contributes a constant expansion coefficient above room temperature. The higher Debye temperature term only reaches saturation (1.15×10^{-5} K^{-1}) by $\sim$ 800 K. The polyhedral volumes are given by $a^3/6$ for the octahedral site (ZrO_6) and $5a^3/6$ for the dodecahedral site (BaO_{12}), and hence, both have the identical polyhedral expansion coefficient to the volume expansivity of the unit cell.

First-order Raman scattering is symmetry-forbidden from the aristotype crystal structure of perovskite, although, as stated earlier, the Raman spectrum has been experimentally measured and characterised [21, 22]. To our knowledge, a high-pressure study of the Raman spectrum of $BaZrO_3$ has not yet been performed, and hence, we lack experimental measurements of the mode Grüneisen parameters of $BaZrO_3$ to make comparisons with the two values derived from the heat capacity/unit cell volume fitting.

Atomic displacement parameters

The temperature dependence of the isotropic atomic displacement parameters for the cations, the anisotropic and the isotropic equivalent atomic displacement parameter for the anion is shown in Fig. 4. All data exhibit the expected variation with temperature, saturation at low temperature and a linear temperature dependence at higher temperatures. For a Debye oscillator, the temperature variation of the mean square displacement is given by [38]

$$\overline{u^2}(T) = \frac{3h^2T}{4\pi^2 M k_B \theta_D^2}\int_0^{\theta_D/T}\frac{x\mathrm{d}x}{\mathrm{e}^x - 1} + \frac{3h^2}{16\pi^2 M k_B \theta_D}$$

where M is the mass of the atomic species under consideration. In practice, the zero-point term is too constrained as it only depends on the vibrational Debye temperature θ_D, and to take account of any static disorder that may also be present, an additional constant is added to the fitting procedure. The full lines shown in Fig. 4 show fits to the temperature variation of the atomic displacement parameters based on this modified Debye model [39]; the fitted values of the vibrational Debye temperatures and the static displacement terms are listed in Table 4. Consideration of the Table 4 shows that the transverse vibrational Debye temperature associated with the anion is significantly higher than that of the barium cation in the large dodecahedral cavity site. The vibrational Debye temperature of the zirconium cation in the constrained octahedral site is significantly higher than that of the barium cation, but still less than that associated with the anion in the isotropic equivalent approximation. The average of the cation vibrational Debye temperatures, 325 K, and that associated with the isotropic equivalent atomic displacement of the anion, 743 K, are well separated and are similar to those resulting from the fitting of the unit cell volume and isochoric heat capacity, 220 K, and 730 K.

Thermodynamic Grüneisen parameter

The thermodynamic Grüneisen parameter (γ_{th}) for $BaZrO_3$ was calculated for the temperature interval 2–500 K using the standard definition $\gamma_{th}(T) = (\alpha_V(T)K_0V_m(T))/c_V(T)$ [34, 40], with the temperature variation of the molar volume, the isochoric heat capacity and the volume expansivity derived from the fitting coefficients; in the absence of experimental data, the bulk modulus was assumed to be constant. The temperature evolution of γ_{th} is illustrated in Fig. 5 and shows only a small dynamic range, decreasing from $\sim$ 1.439 at 2 K to $\sim$ 1.398 at 500 K in good agreement with the weighted mean of the individual Grüneisen constants derived from the two-term Debye fitting to the volume and isochoric heat capacity. Assuming Dulong–Petit behaviour for the isochoric heat capacity and the high-temperature volume expansivity deduced from the fitting procedure, at high temperatures $\gamma_{th}(T) \sim 1.6 \times 10^{-7}$ $K_0(T)V_m(T) \sim 1.36$.

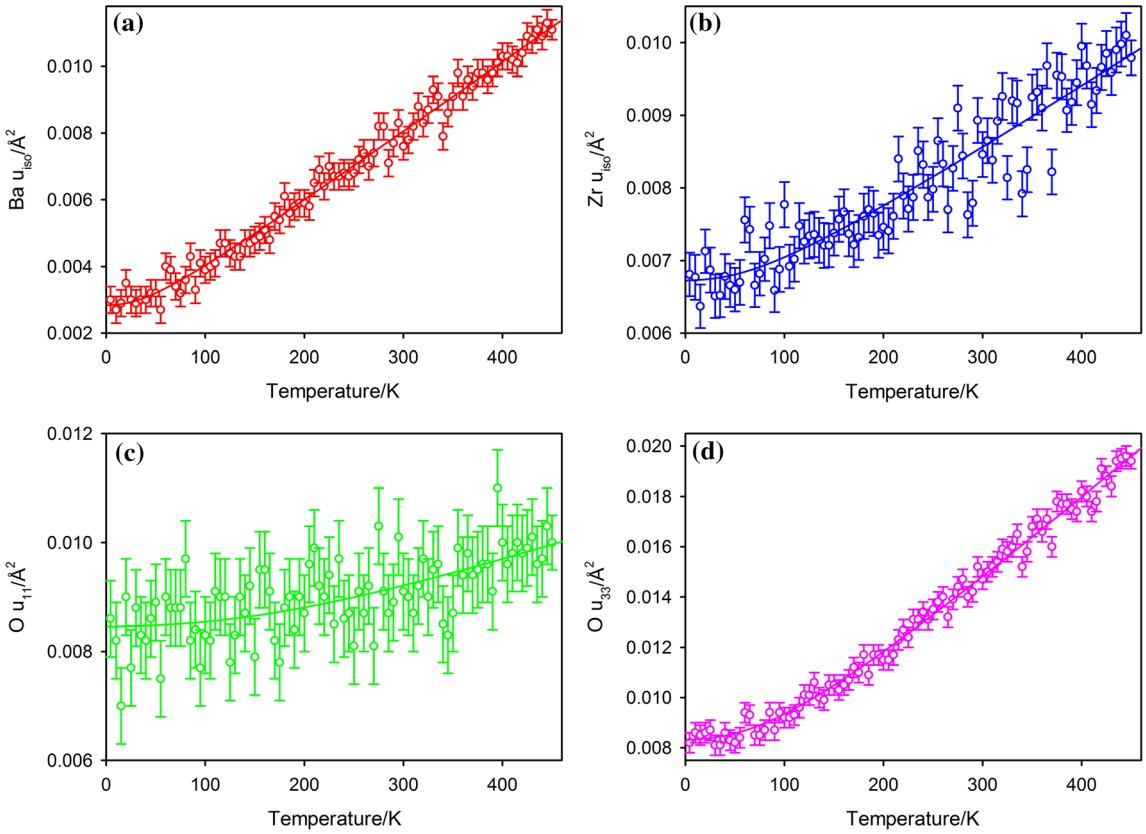

Figure 4 The temperature dependence of the isotropic atomic displacement parameters for the cations and the anisotropic atomic displacement parameters for the oxygen anion. Full lines show the fits to these data based on the modified Debye model described in the text.

Table 4 Vibrational Debye temperatures and mean square static disorder in $BaZrO_3$

Atom	Vibrational Debye temperature/K	Mean square static disorder/Å^2
Ba	224(1)	$1.65(6) \times 10^{-3}$
Zr	426(7)	$5.79(7) \times 10^{-3}$
O u_{11}	1188(54)	$6.6(2) \times 10^{-3}$
O u_{33}	521(2)	$3.93(7) \times 10^{-3}$
$1/3(u_{11} + 2u_{33})$	743(54)	
O u_{eq}	604(11)	$4.6(1) \times 10^{-3}$

Discussion and conclusions

In the temperature interval 4.2–450 K, high-resolution time-of-flight neutron powder diffraction has shown $BaZrO_3$ to be cubic with the aristotype crystal structure. No evidence was found for the tetragonal distortion of the unit cell predicted by ab initio calculations which would be expected to maximise at the lowest temperature assuming critical behaviour of the ZrO_6 octahedral rotation angle. Furthermore, no evidence was found for diffuse scattering at the R point superlattice positions of the cubic Brillouin zone. Analysis of the temperature evolution of the unit cell volume and the isochoric heat capacity is consistent with a simple thermodynamic model that treats $BaZrO_3$ perovskite as a two-term Debye system with separated cation and anion behaviour. Characteristic temperatures derived from simultaneous fitting of the heat capacity and volume are found to be in fair to good agreement with the vibrational Debye temperatures derived from fitting the temperature dependence of the atomic displacement parameters. Assessment of the vibrational Debye temperatures of the cations when compared to the lower

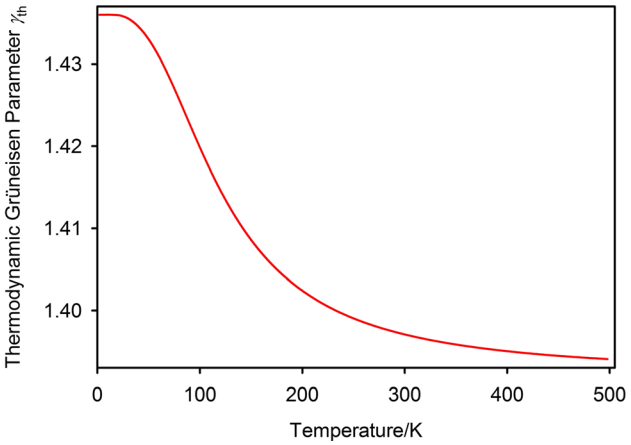

Figure 5 The temperature variation of the thermodynamic Grüneisen parameter for $BaZrO_3$.

characteristic temperature showed poorer agreement for the octahedrally coordinated zirconium cation compared to the 12-fold-coordinated barium cation. However, a re-evaluation of the isochoric heat capacity/volume fitting to a three-term Debye model, allowing the two cations to be associated with independent Debye temperatures, did not improve the quality of fit to these data and hence was rejected on statistical grounds.

The simultaneous fitting of the isochoric heat capacity and unit cell volume to the two-term Debye model has been applied successfully to a number of other oxide and fluoride perovskite-structured compounds ($SrZrO_3$ [25], $BaCeO_3$ [26], $CaTiO_3$ [41], $LaGaO_3$ [24], $KZnF_3$ [42], $KCaF_3$ [43]). From these results, a vibrational density of states (VDOS) can be evaluated from the two Debye cut-off frequencies for comparison with either direct measurements of the phonon dispersion curves or sophisticated ab initio calculations. Despite the simplicity of the model, for the case of $KZnF_3$ [42], good agreement was found for the equivalence of the higher characteristic temperature equating to the high-frequency cut-off in the experimental VDOS and the lower characteristic temperature corresponding to the mean frequency of the total VDOS. Unfortunately, we lack either an experimental or calculated VDOS for $BaZrO_3$ to make this comparison.

There are disappointingly few detailed low-temperature crystallographic studies of perovskite-structured compounds with either barium in the cavity site or zirconium in the octahedral site. To compare and contrast the thermal behaviour of $BaZrO_3$, we are limited to the two compounds that have been studied in sufficient detail: $BaCeO_3$ [26] and $SrZrO_3$ [25]. These results are summarised in Fig. 6 where the temperature dependences of the normalised unit cell volume, the volume expansivity, the normalised polyhedral volumes and the atomic displacement parameters of barium and zirconium are illustrated. Between 1.2 and 500 K, both $BaCeO_3$ and $SrZrO_3$ are orthorhombic, space group *Pbnm* with the alkaline earth in eightfold coordination [26, 44]. Both phases exhibit octahedral tilting [19] and undergo a series of structural phase transitions with increasing temperature to reach the untilted cubic aristotype crystal structure exhibited by $BaZrO_3$ ($BaCeO_3$ 563 K to *Ibnn*, 673 K to $F\bar{3}2/n$ 1173 K to $Pm\bar{3}m$ [45], $SrZrO_3$ 973 K to *Imma*, 1103 K to *I*4/*mcm*, 1443 K to $Pm\bar{3}m$[44]). For perovskite-structured materials that crystallise with the aristotype structure, thermal expansion can only occur through an increase in the dodecahedral–anion and octahedral–anion bond lengths. This contrasts with crystal structures based on zone-boundary tilting of the octahedra where the untilting of the octahedra with increasing temperature makes a significantly greater contribution to the volume expansivity than the bond length increase. For both $BaCeO_3$ and $SrZrO_3$, the transition from the lowest temperature phase to the next highest is tricritical in nature [25, 26], and hence, as the Ce–O bond length is larger than the Zr–O bond length, we expect the volume expansion coefficients to be in the order $BaCeO_3$, $SrZrO_3$, $BaZrO_3$, which is as measured (Fig. 6a).

The untilting of the CeO_6 octahedra increases the polyhedral volume of the irregular BaO_8 site in $BaCeO_3$ due to the large magnitude of the Ce–O bond length, whereas the polyhedral volume of the dodecahedral BaO_{12} site in $BaZrO_3$ is governed by the temperature variation of the Ba–O bond length. The normalised polyhedral volume change of the barium site in $BaCeO_3$ is therefore significantly larger than that in $BaZrO_3$ (Fig. 6b). Whilst the volume of the cavity site in most perovskite-structured compounds is found to increase with increasing temperature, the volume of the octahedral site in zone-boundary-tilted crystal structures is more subtle. For $BaZrO_3$, the octahedral volume expansivity is identical to that of the unit cell volume, i.e. increases with increasing temperature; however, in $SrZrO_3$, the ZrO_6 octahedral expansivity is found to be negative

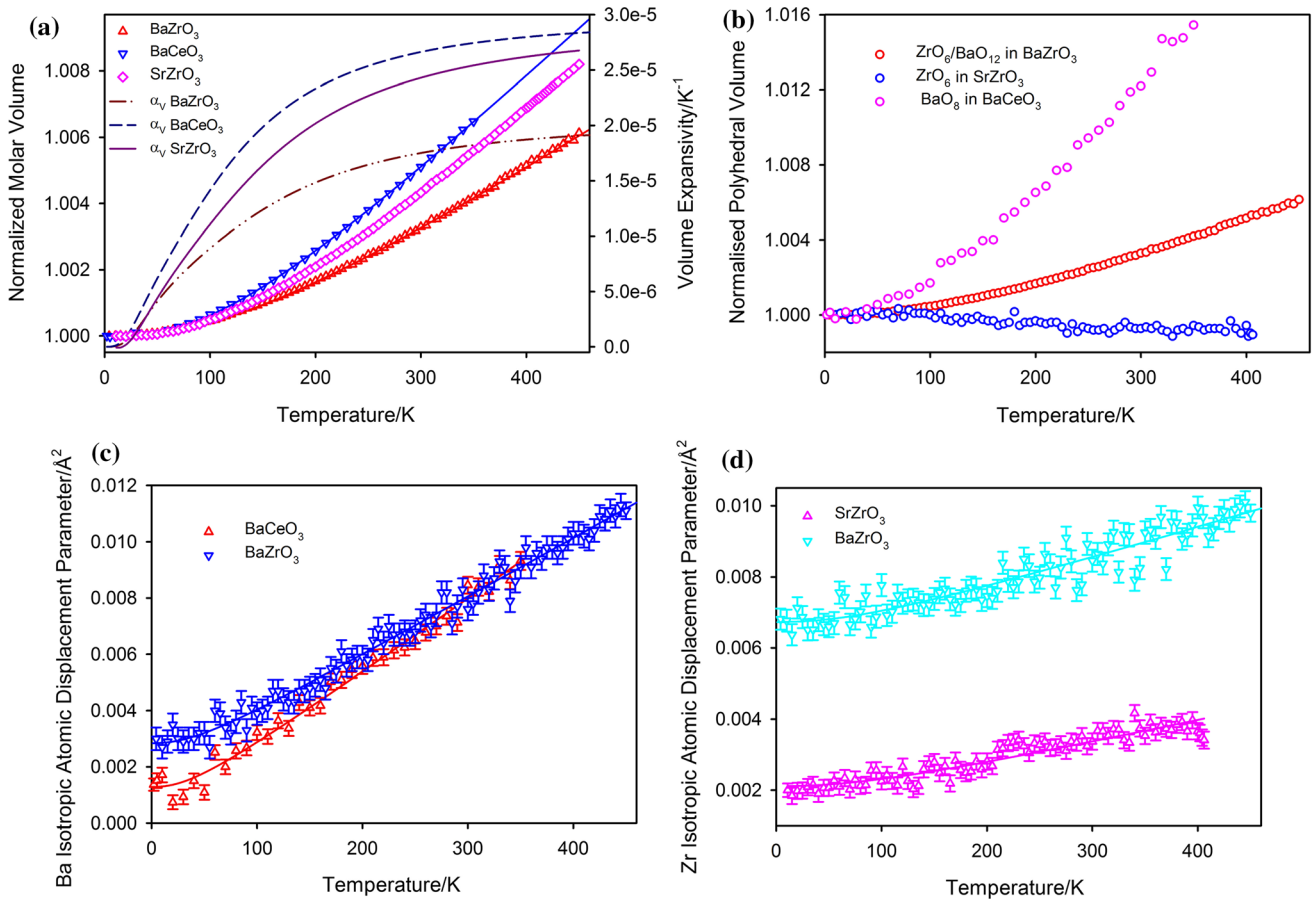

Figure 6 Comparison of the temperature dependences of the crystallographic parameters of $BaZrO_3$ with $BaCeO_3$ (Ba in the cavity site) and $SrZrO_3$ (Zr in the octahedral site). **a** Normalised molar volumes and calculated volume expansion coefficients derived from two-term fitting coefficients. **b** Normalised polyhedral volumes. **c** Isotropic atomic displacement parameter for Ba in the modified Debye model. **d** Isotropic atomic displacement parameter for Zr in the modified Debye model.

(Fig. 6b) with the magnitude of the normalised volume of the ZrO_6 octahedron in $SrZrO_3$ being smaller than that determined for $BaZrO_3$.

The atomic displacement parameters for the barium cation in both $BaCeO_3$ and $BaZrO_3$ are similar in magnitude and temperature dependence with the vibrational Debye temperature of $BaZrO_3$ (224(1) K) only marginally larger than $BaCeO_3$ (200(2) K) [26] (Fig. 6c). By contrast, the atomic displacement parameters for the zirconium cation in $BaZrO_3$ and $SrZrO_3$ are significantly different in magnitude but exhibit a similar temperature dependence with the vibrational Debye temperature of $SrZrO_3$ (499(9) K) [25] exceeding that of $BaZrO_3$ (426(7) K) (Fig. 6d). Estimates of the static disorder for the zirconium site in $BaZrO_3$ are approximately 4.5 times larger than the corresponding site in $SrZrO_3$, possibly suggesting the presence of eightfold systematic disorder as observed in $BaTiO_3$ [46].

The recently reported float-zone growth of large single crystals of $BaZrO_3$ [47] would be ideal for a single crystal neutron diffuse scattering study that would permit investigation of any positional disorder of the zirconium site and also the investigation of the proposed glassy structural state.

Acknowledgements

I am grateful for the rapid review of this manuscript and the suggestions of the reviewers that have been incorporated and have improved this article. This paper is dedicated to the memory of my friend Sten-Gunnar Eriksson (1958–2018), solid state chemist and crystallographer, formerly of the Department of Chemistry and Chemical Engineering, Chalmers

University of Technology, Gothenburg, Sweden. Mr R A Major (ISIS Facility) is thanked for technical support during this experiment.

Compliance with ethical standards

Conflict of interest The author declares he has no conflict of interest.

References

[1] Mitchell RH (2002) Perovskites modern and ancient. Almaz Press, Thunder Bay

[2] Megaw HD (1973) Crystal structures, a working approach. Saunders, London

[3] Akbarzadeh AR, Kornev I, Malibert C, Bellaiche L, Kiat JM (2005) Combined theoretical and experimental study of the low-temperature properties of $BaZrO_3$. Phys Rev B 72:205104

[4] Nagarajan K, Saha R, Babu R, Mathews CK (1985) Thermodynamic functions of barium and strontium zirconates from calorimetric measurements. Thermochim Acta 90:297–304

[5] Takashi T, Iwahara H (1980) Solid state ionics: proton conduction in perovskite type solid solutions. Rev Chim Miner 17:243–253

[6] Ahmed I, Eriksson S-G, Ahlberg E, Knee CS, Karlsson M, Matic A, Engberg D, Börjesson L (2006) Proton conductivity and low temperature structure of In-doped $BaZrO_3$. Solid State Ion 177:2357–2362

[7] Ishihara T (2009) Perovskite oxide for solid oxide fuel cells. Springer, Boston

[8] Liu W, Ren X (2009) Large piezoelectric effect in Pb-free ceramics. Phys Rev Lett 103:257602

[9] Zhao Y, Weidner DJ (1991) Thermal expansion of $SrZrO_3$ and $BaZrO_3$ perovskites. Phys Chem Miner 18:294–301

[10] Saha R, Babu R, Nagarajan K, Mathews CK (1989) Thermodynamic properties of ternary oxides of fission products from calorimetric measurements. J Nucl Mater 167:271–277

[11] Saha R, Babu R, Nagarajan K, Mathews CK (1987) Thermodynamic properties of compounds of alkaline earth elements with other fission products. Thermochim Acta 120:29–39

[12] Yamanaka S, Kurosaki K, Maekawa T, Matsuda T, Kobayashi S-I, Uno M (2005) Thermochemical and thermophysical properties of alkaline-earth perovskites. J Nucl Mater 344:61–66

[13] Yamanaka S, Fujikane M, Hamaguchi T, Muta H, Oyama T, Matsuda T, Kobayashi S-I, Kurosaki K (2003) Thermophysical properties of $BaZrO_3$ and $BaCeO_3$. J Alloys Compd 359:109–113

[14] Yamanaka S, Hamaguchi T, Oyama T, Matsuda T, Kobayashi S-I, Kurosaki K (2003) Heat capacities and thermal conductivities of perovskite type $BaZrO_3$ and $BaCeO_3$. J Alloys Compd 359:1–4

[15] Koizumi M, Satoh M, Noro K (1974) Phase study on solid fission products, Ba, Sr and Zr in oxide fuel. J Nucl Mater 51:90–94

[16] Amaroso D, Cano A, Ghosez P (2018) First-principles study of (Ba, Ca)TiO_3 and Ba(Ti, Zr)O_3 solid solutions. Phys Rev B 97:174108

[17] Lebedev AI, Sluchinskaya IA (2013) Structural instability in $BaZrO_3$ crystals: calculations and experiment. Phys Solid State 55:1941–1945

[18] Bennet JW, Grinberg I, Rappe AM (2006) Effect of symmetry lowering on the dielectric response of $BaZrO_3$. Phys Rev B 73:180102

[19] Glazer AM (2011) A brief history of tilts. Phase Transit 84:405–420

[20] Bilić A, Gale JD (2009) Ground state structure of $BaZrO_3$: a comparative first-principles study. Phys Rev B 79:174107

[21] Giannici F, Shipour M, Longo A, Martorana A, Merkle R, Maier J (2011) Long-range and short-range structure of proton-conducting Y:$BaZrO_3$. Chem Mater 23:2994–3002

[22] Shi F, Dong H, Liu Q, Yang J, Ren S, Sun H, Xiong J (2017) Investigation and theoretical calculation of the lattice vibrational spectra of $BaZrO_3$ ceramic. J Mater Sci Mater Electron 28:3467–3473

[23] Yang X, Li Q, Liu R, Liu B, Zhang H, Jiang S, Liu J, Zou B, Cui T, Liu B (2014) Structural phase transition of $BaZrO_3$ under high pressure. J Appl Phys 115:124907

[24] Knight KS (2012) Low temperature thermoelastic and structural properties of $LaGaO_3$ perovskite in the *Pbnm* phase. J Solid State Chem 194:286–296

[25] Knight KS, Bull CL (2016) Low temperature and high pressure thermoelastic and crystallographic properties of $SrZrO_3$ perovskite in the *Pbnm* phase. Solid State Sci 62:90–104

[26] Knight KS, Bonanos N (2013) Thermoelastic and structural properties of ionically conducting cerate perovskites:(I) $BaCeO_3$ at low temperatures in the *Pbnm* phase. Solid State Ion 232:112–122

[27] Fortes AD (2018) Accurate and precise lattice parameters of H_2O and D_2O ice Ih between 1.6 and 270 K from high-resolution time-of-flight neutron powder diffraction data. Acta Crystallogr B 74:196–216

[28] Sears VF (1992) Neutron scattering lengths and cross sections. Neutron News 3:26–37

[29] Von Dreele RB, Larson AC (1986) GSAS. Los Alamos National Laboratory Report LAUR 86-748

[30] Reif F (1965) Fundamentals of statistical and thermal physics. McGraw-Hill, New York

[31] Mathews MD, Mirza EB, Momin AC (1991) High-temperature X-ray diffractometric studies of $CaZrO_3$, $SrZrO_3$ and $BaZrO_3$. J Mater Sci Lett 10:305–306

[32] Han D, Hatada N, Uda T (2016) Chemical expansion of yttrium-doped barium zirconate and correlation with proton concentration and conductivity. J Am Ceram Soc 99:3745–3753

[33] Taglieri G, Tersigni M, Villa PL, Mondelli C (1999) Synthesis by the citrate route and characterisation of $BaZrO_3$ a high tech ceramic oxide:preliminary results. Int J Inorg Mater 1:103–110

[34] Wallace DC (1972) Thermodynamics of crystals. Wiley, New York

[35] Ahrens M, Maier J (2006) Thermodynamic properties of $BaCeO_3$ and $BaZrO_3$ at low temperatures. Thermochim Acta 443:189–196

[36] Barron THK (1998) generalised theory of thermal expansion of solids. CINDAS Data Ser Mater Prop 1–4:1–108

[37] Terki R, Feraoun H, Bertrand G, Aourag H (2005) Full potential calculation of structural, elastic and electronic properties of $BaZrO_3$ and $SrZrO_3$. Phys State Solidi (b) 242:1054–1062

[38] James RW (1962) The optical principles of the diffraction of X-rays. Bell, London

[39] Wood IG, Knight KS, Price GD, Stuart JA (2002) Thermal expansion and atomic displacement parameters of cubic $KMgF_3$ perovskite determined by high-resolution neutron powder diffraction. J Appl Crystallogr 35:291–295

[40] Barron THK, White GK (1999) Heat capacity and thermal expansion at low temperatures. Kluwer Academic, New York

[41] Knight KS (2011) Structural and thermoelastic properties of $CaTiO_3$ perovskite between 7 K and 400 K. J Alloys Compd 509:6337–6345

[42] Knight KS, Bull CL, McIntyre P (2017) Low temperature, high pressure thermo-physical and crystallographic properties of $KZnF_3$ perovskite. Mater Chem Phys 199:393–407

[43] Knight KS (2017) High-pressure thermoelastic and structural properties of $KCaF_3$ perovskite in the low temperature *Pbnm* phase. J Alloys Compd 693:1305–1314

[44] Howard CJ, Knight KS, Kennedy BJ, Kisi EH (2000) Structural phase transitions in $SrZrO_3$ revisited. J Phys Condens Mat 12:L677–L683

[45] Knight KS (1994) Structural phase transitions in $BaCeO_3$. Solid State Ion 94:109–117

[46] Ravel B, Stern EA, Vedrinskii RI, Kraizman V (1998) The local structure and phase transitions of $BaTiO_3$. Ferroelectrics 206–207:407–430

[47] Xin C, Veber P, Guennou M, Toulouse C, Valle N, Ciomaga Hatnean M, Balakrishnan G, Haumont R, Saint Martin R, Velazquez M, Alain Maillard A, Rytz D, Josse M, Maglione M, Kreisel J (2019) Single crystal growth of $BaZrO_3$ from the melt at 2700 °C using optical floating zone technique and growth prospects from BaB_2O_4 flux at 1350 °C. CrystEngComm 21:502–512